Transient soil-structure interaction with consistent description of radiation damping

Ediansjah Zulkifli[†] and Peter Ruge

Lehrstuhl Dynamik der Tragwerke, Fakultät Bauingenieurwesen, Technische Universität Dresden, D-01062 Dresden, Germany

Abstract. Radiation damping due to wave propagation in unbounded domains may cause a significant reduction of structural vibrations when excited near resonance. Here a novel matrix-valued algebraic Padé-like stiffness formulation in the frequency-domain and a corresponding state equation in the time domain are elaborated for a soil-structure interaction problem with a layered soil excited in a transient manner by a flexible rotor during startup and shutdown. The contribution of radiation damping caused by a soil-layer upon a rigid bedrock is characterized by the corresponding amount of critical damping as it is used in structural dynamics.

Keywords: boundary element method; soil dynamics; frequency-to-time transformation; radiation damping; soil-structure interaction.

1. Introduction

There is a wide range of dynamic problems in engineering where infinite or semi-infinite media are involved. For such systems effects from propagating waves in water, air or elastic solids cannot be neglected in analysis.

Fig. 1 shows a typical setup of a soil-structure interaction problem with a rotating machine which causes transients at startup or shutdown. In this case, waves will emit from the foundation and may lead to a reduction of the structural response and thus causes a kind of damping called radiation damping.

The example of soil-structure interaction above can be treated by splitting the system into two distinct parts: near field (the structure, which may also include some portion of the soil) and far field (unbounded soil). This method is taken form substructure technique, which has been introduced by Vaish and Chopra (1974). Typically, the structure together with an irregular adjacent soil region is treated by finite element method (FEM) which may behave non-linearly. Extensive research was conducted to describe the unbounded soil with an analytical or semi-analytical methods. A comprehensive review of the soil-structure interaction problem particularly with computational methods is given by Antes and Spyrakos (1996).

In this paper, an alternative method to represent an unbounded soil in a dynamic analysis is

---

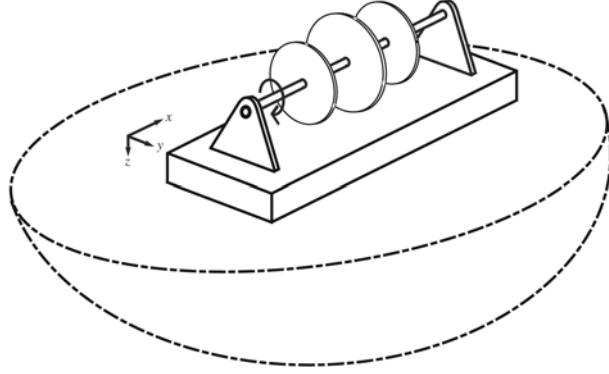† Ph.D., Corresponding author, E-mail: Ediansjah.Zulkifli@tu-dresden.de

Fig. 1 Rotor on a foundation plate resting on the halfspace

presented. A special emphasis is placed on a consistent description of radiation damping in the time-domain. A main purpose of the developed strategy is to find a formulation applicable to transient excitation problems. In principle, it is a combination of the boundary element method (BEM) in the frequency domain to reproduce the far-field and the FEM in the time domain to analyze the near-field. This alternative procedure avoids the introduction of any artificial non reflecting boundaries.

The procedure is based on a rational approximation of the dynamical stiffness of the unbounded domain in the frequency-domain. Here, discrete values of the dynamical stiffness are interpolated by means of continuous rational functions. This idea was originally proposed by Wolf (1991, 1994) for the scalar wave equation only in order to represent the soil by a simple physical model. In a series of papers Ruge and Trinks (2002, 2003), Ruge *et al.* (2001, 2006), extended this interpolation by a continuous rational form of $\mathbf{K}(\omega)$ to multiple degrees of freedom, and it has been implemented in the works of Trinks and Ruge (2002a, 2003b, 2002b, 2003a), Trinks *et al.* (2001a,b), Trinks (2005) and Zulkifli (2008).

Hence, the state variables $\mathbf{u}_c(t)$ (nodal displacements) and the nodal forces $\mathbf{f}_c(t)$ in the interface are related by the frequency dependent dynamic stiffness matrix $\mathbf{K}(\omega)$ assuming a harmonic behavior in the time domain

$$\left. \begin{aligned} \mathbf{f}_c(t) &= \hat{\mathbf{f}}_c e^{(i\omega t)} \\ \mathbf{u}_c(t) &= \hat{\mathbf{u}}_c e^{(i\omega t)} \end{aligned} \right\} \quad \hat{\mathbf{f}}_c(\omega) = \mathbf{K}(\omega)\hat{\mathbf{u}}_c \tag{1}$$

A set of $\mathbf{K}_j = \mathbf{K}(\omega_j)$ found numerically or analytically is then used to establish a matrix-valued interpolation form of $\mathbf{K}(\omega)$, that is

$$\mathbf{K}(\omega) = \mathbf{Q}^{-1}(\omega)\mathbf{P}(\omega) \tag{2}$$

where $\mathbf{Q}$ and $\mathbf{P}$ are matrix polynomials

$$\mathbf{Q}(\omega) = \mathbf{Q}_0 + (i\omega)\mathbf{Q}_1 + (i\omega)^2\mathbf{Q}_2 + \ldots + (i\omega)^M\mathbf{Q}_M$$

$$\mathbf{P}(\omega) = \mathbf{P}_0 + (i\omega)\mathbf{P}_1 + (i\omega)^2\mathbf{P}_2 + \ldots + (i\omega)^{M+1}\mathbf{P}_{M+1} \tag{3}$$

with *M* is the approximation order of the dynamic stiffness.

A limited range of ω is used for the approximation process, corresponding with a finite number of dynamical stiffness matrices. The matrix-valued coefficients of the rational approximation function are determined by means of a least-square procedure. Explicit details of how to obtained $\mathbf{P}$ and $\mathbf{Q}$ in the above equation can be found in Ruge *et al.* (2001). The dynamic stiffness matrix $\mathbf{K}(\omega)$ has to be known either analytically or it must be numerically obtained for each given value of ω. In this paper, the numerical results for the dynamic stiffness of soil $\mathbf{K}(\omega)$ is obtained from a Boundary Element approach in the frequency domain.

2. BEM in elastodynamics

In elastodynamics, the Navier differential equation of motion of an isotropic, homogenous viscoelastic medium is wellknown

$$(c_p^2 - c_s^2)u_{j,ij} + c_s^2 u_{i,jj} + \frac{b_i}{\rho} = \ddot{u}_i \tag{4}$$

where ρ is the mass density, b is the body force per unit mass, u_j is the displacement field, c_p is the propagation speed of longitudinal waves and c_s for the transversal waves

$$c_p^2 = \frac{E(1-\nu)}{\rho(1+\nu)(1-2\nu)}, \quad c_s^2 = \frac{E}{2\rho(1+\nu)} \tag{5}$$

or in terms of shear modulus G

$$c_p^2 = \frac{2G(1-\nu)}{\rho(1-2\nu)}, \quad c_s^2 = \frac{G}{\rho} \tag{6}$$

where E is Young's modulus and ν is Poisson's ratio.

The exact harmonic solution $u(\mathbf{x}, t) = \hat{u}(\mathbf{x}, \omega)e^{i\omega t}$ in the time-domain transforms the motion Eq. (4) into the frequency-domain

$$(c_p^2 - c_s^2)\hat{u}_{j,ij} + c_s^2 \hat{u}_{i,jj} + \frac{\hat{b}_i}{\rho} = -\omega^2 \hat{u}_i \tag{7}$$

In the absence of body forces, the domain Eq. (7) can be expressed as surface equation by using Somigliana's Identity based on Betti's reciprocal theorem

$$u_i(\xi) = \int_\Gamma u_{ij}^*(\mathbf{x}, \xi)p_j(\mathbf{x})d\Gamma - \int_\Gamma p_{ij}^*(\mathbf{x}, \xi)u_j(\mathbf{x})d\Gamma \tag{8}$$

where ξ is the source point where a unit force is applied and $\mathbf{x}$ is the observation point at the surface Γ. u_j and p_j are the physical displacements and surface traction in the j direction. u_{ij}^* and p_{ij}^* correspond to the fundamental solutions in the j direction due to point load applied in the i direction. Details of these fundamental solutions in elastodynamics can be found in Bausinger and Kuhn (1987), Andersen and Jones (2001) and Beskos (1987).

The integral equation for a point on the surface Γ can be derived from Eq. (8)

$$c_{ij}(\xi)u_j(\xi) + \int_\Gamma p_{ij}^*(\mathbf{x}, \xi)u_j(\mathbf{x})d\Gamma = \int_\Gamma u_{ij}^*(\mathbf{x}, \xi)p_j(\mathbf{x})d\Gamma \tag{9}$$

The above integrals are in the sense of Cauchy principal values; when Γ is assumed to be smooth at 'ξ' then c_{ij} simplifies to $c_{ij}(\xi) = \frac{1}{2}\delta_{ij}$. For any other surface geometry at the source point, other values of $c_{ij}(\xi)$ are obtained. Discussion of the values of $c_{ij}(\xi)$ for various surface conditions can be found in Hartmann (1981).

In order to solve the boundary integral equations numerically, the boundary has to be discretized into a series of elements over which displacements and traction are written in terms of their values at a series of nodal points. The displacement and traction fields are interpolated over each element using a set of shape functions, which are also used to approximate the geometry.

Rewriting the Eq. (9) in a discretized form creates a system of linear algebraic equations

$$\mathbf{C}(\xi)\mathbf{U}_j + \sum_{k=1}^{NE}\left\{\int_{\Gamma_k}\mathbf{P}^*(\mathbf{x},\xi)\Phi_k(\mathbf{x})d\Gamma_k\right\}\mathbf{U}_k = \sum_{k=1}^{NE}\left\{\int_{\Gamma_k}\mathbf{U}^*(\mathbf{x},\xi)\Phi_k(\mathbf{x})d\Gamma_k\right\}\mathbf{P}_k \tag{10}$$

where NE is the number of boundary elements in the domain and $\Phi_k(\mathbf{x})$ is an element shape function. In this paper, all of the soil surfaces were discretized into nine-node Lagrange element with quadratic shape functions presented in Cook *et al.* (1989).

Altogether N source points generate a global matrix equation for the entire domain

$$\left[\underset{3N\times 3N}{\hat{\mathbf{C}}} + \underset{3N\times 3N}{\hat{\mathbf{H}}}\right]\underset{3N\times 1}{\mathbf{U}} = \underset{3N\times 3N}{\mathbf{G}}\ \underset{3N\times 1}{\mathbf{P}} \tag{11}$$

The matrix $\hat{\mathbf{C}}$ stores the (3×3) matrices $\mathbf{C}(\xi)$ for each of the observation nodes along the diagonal. Introducing $\mathbf{H} = \hat{\mathbf{C}} + \hat{\mathbf{H}}$, the Eq. (11) can be written like

$$\underset{3N\times 3N}{\mathbf{H}}\ \underset{3N\times 1}{\mathbf{U}} = \underset{3N\times 3N}{\mathbf{G}}\ \underset{3N\times 1}{\mathbf{P}} \tag{12}$$

where the matrices $\mathbf{H}$ and $\mathbf{G}$ have to be calculated for each value of ω, since the fundamental solution depends on the frequency.

The integration process is accomplished with a standard Gauss-Legendre quadrature if the source point does not lie in the element. Matrix $\mathbf{G}$ contains terms with singularities of type $1/r$ when the source point lies in the element. To overcome this situation, Li *et al.* (1985) proposed a method based on a transformation of the integration area.

Matrix $\mathbf{H}$ contains terms with singularities of type $1/r^2$ when the observation point coincides with the source point. This situation is treated with a rigid body assumption for a closed, interior domain where no traction appear on any part of the surface. For a halfspace problem with no closed domain an artificial, enclosing boundary (enclosing elements) is constructed (Ahmad and Banerjee 1988).

3. Transformation into the time-domain

The description in the frequency domain is established by means of (2) and (3)

$$\hat{\mathbf{f}}_c = [\mathbf{Q}(\omega)]^{-1}[\mathbf{P}(\omega)]\hat{\mathbf{u}}_c,$$
$$= [\mathbf{Q}_0 + i\omega\mathbf{Q}_1 + \ldots + (i\omega)^M\mathbf{Q}_M]^{-1}[\mathbf{P}_0 + i\omega\mathbf{P}_1 + \ldots + (i\omega)^{M+1}\mathbf{P}_{M+1}]\hat{\mathbf{u}}_c \tag{13}$$

In order to achieve a pure linear formulation with respect to $(i\omega)$ instead of the rational form in (13), a special algebraic splitting process is introduced. In a first step the fraction in Eq. (13) is

replaced by a linear part $[\mathbf{S}_0^0 + (i\omega)\mathbf{S}_1^{(0)}]$ and a strictly proper rational function of reduced order

$$\hat{\mathbf{f}}_c = [\mathbf{S}_0^0 + (i\omega)\mathbf{S}_1^{(0)}]\hat{\mathbf{u}}_c +$$

$$\underbrace{[\mathbf{Q}_0 + i\omega\mathbf{Q}_1 + \ldots + (i\omega)^M\mathbf{Q}_M]^{-1}[\mathbf{R}_0^{(0)} + i\omega\mathbf{R}_1^{(0)} + \ldots + (i\omega)^{M-1}\mathbf{R}_{M-1}^{(0)}]\hat{\mathbf{u}}_c}_{\hat{\mathbf{v}}_1} \qquad (14)$$

The matrices $\mathbf{S}_0$, $\mathbf{S}_1$ and $\mathbf{R}_i$ are obtained by comparing coefficients at powers of $(i\omega)$. The remaining rational part is taken to define an additional variable $\hat{\mathbf{v}}_1$. This definition for $\hat{\mathbf{v}}_1$ is formulated in 'inverse manner' as the next step

$$\hat{\mathbf{v}}_1 = [\mathbf{Q}(\omega)]^{-1}[\mathbf{R}(\omega)]\hat{\mathbf{u}}_c$$

$$= [\mathbf{Q}_0 + i\omega\mathbf{Q}_1 + \ldots + (i\omega)^M\mathbf{Q}_M]^{-1}[\mathbf{R}_0^{(0)} + i\omega\mathbf{R}_1^{(0)} + \ldots + (i\omega)^{M-1}\mathbf{R}_{M-1}^{(0)}]\hat{\mathbf{u}}_c$$

$$\Downarrow \qquad\qquad\qquad (15)$$

$$\hat{\mathbf{u}}_c = [\mathbf{R}(\omega)]^{-1}[\mathbf{Q}(\omega)]\hat{\mathbf{v}}_1$$

$$= [\mathbf{R}_0^{(0)} + i\omega\mathbf{R}_1^{(0)} + \ldots + (i\omega)^{M-1}\mathbf{R}_{M-1}^{(0)}]^{-1}[\mathbf{Q}_0 + i\omega\mathbf{Q}_1 + \ldots + (i\omega)^M\mathbf{Q}_M]\hat{\mathbf{v}}_1$$

The splitting process outlined in (14) is repeated, and the improper fractional part in (15) is replaced with a subsequence linear part $[\mathbf{S}_0^{(1)} + (i\omega)\mathbf{S}_1^{(1)}]$

$$\hat{\mathbf{u}}_c = [\mathbf{S}_0^{(1)} + (i\omega)\mathbf{S}_1^{(1)}]\hat{\mathbf{v}}_1 +$$

$$\underbrace{[\mathbf{R}_0^{(0)} + i\omega\mathbf{R}_1^{(0)} + \ldots + (i\omega)^{M-1}\mathbf{R}_{M-1}^{(0)}]^{-1}[\mathbf{R}_0^{(1)} + i\omega\mathbf{R}_1^{(1)} + \ldots + (i\omega)^{M-2}\mathbf{R}_{M-2}^{(1)}]\hat{\mathbf{v}}_1}_{\hat{\mathbf{v}}_2} \qquad (16)$$

$$\Updownarrow$$

$$\hat{\mathbf{u}}_c = [\mathbf{S}_0^{(1)} + (i\omega)\mathbf{S}_1^{(1)}]\hat{\mathbf{v}}_1 + \hat{\mathbf{v}}_2 \qquad (17)$$

Again, the splitting process outlined above is repeated. The new additional variable $\hat{\mathbf{v}}_2$ in (17) is replaced with a subsequence linear part $[\mathbf{S}_0^{(2)} + (i\omega)\mathbf{S}_1^{(2)}]$

$$\hat{\mathbf{v}}_2 = [\mathbf{S}_0^{(2)} + (i\omega)\mathbf{S}_1^{(2)}]\hat{\mathbf{v}}_2 + \underbrace{[\mathbf{R}^{(1)}(\omega)]^{-1}[\mathbf{R}^{(2)}(\omega)]\hat{\mathbf{v}}_2}_{\hat{\mathbf{v}}_3} \qquad (18)$$

$$\vdots$$

continuation

with $\mathbf{R}^{(1)}(\omega)$ and $\mathbf{R}^{(2)}(\omega)$ in Eq. (18) represented below

$$\mathbf{R}^{(1)}(\omega) = [\mathbf{R}_0^{(1)} + i\omega\mathbf{R}_1^{(1)} + \ldots + (i\omega)^{M-2}\mathbf{R}_{M-2}^{(1)}]$$

$$\mathbf{R}^{(2)}(\omega) = [\mathbf{R}_0^{(2)} + i\omega\mathbf{R}_1^{(2)} + \ldots + (i\omega)^{M-3}\mathbf{R}_{M-3}^{(2)}]$$

The splitting process procedure is repeated until only a strictly proper part remains whose denominator polynomial is a linear function. Details of this explicit process can be found in Ruge *et al.* (2001).
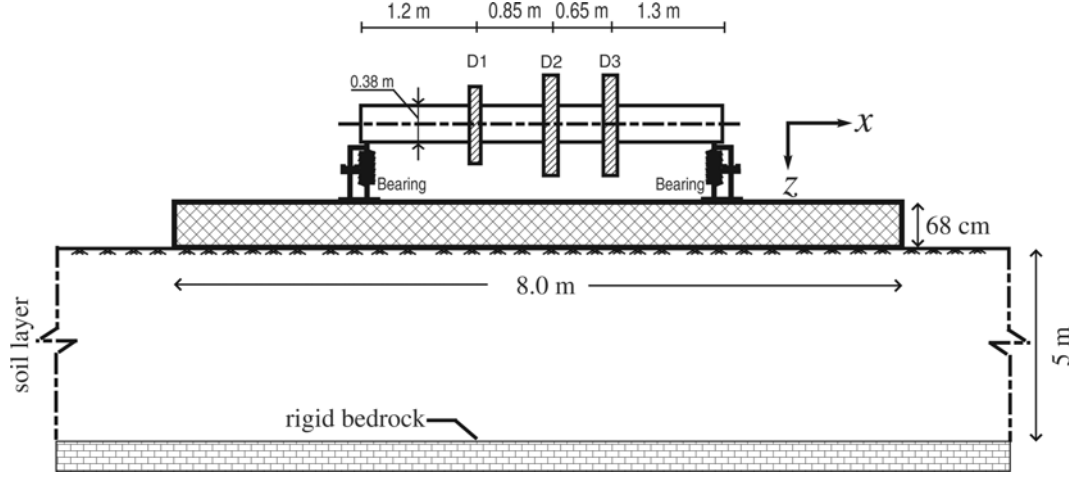
Fig. 2 Side view of gyroscopic rotor on a soil layer over a rigid bedrock

Finally, with N_K indicating the order of the dynamic stiffness matrix $\mathbf{K}(\omega)$, this splitting process results in a strictly linear system of order $(M + 1) \times N_K$. It can be formulated in the spectral-domain as well as in the time-domain.

$$\mathbf{A}\,\hat{\mathbf{u}}(i\omega)\mathbf{B}\,\hat{\mathbf{u}} = \hat{\mathbf{f}} \tag{19a}$$

$$\mathbf{A}\,\mathbf{u}(t) + \mathbf{B}\,\dot{\mathbf{u}}(t) = \mathbf{f}(t); \quad \mathbf{u}(t) = \hat{\mathbf{u}}e^{i\omega t}, \quad \mathbf{f}(t) = \hat{\mathbf{f}}e^{i\omega t} \tag{19b}$$

where the system matrices are strictly banded

$$\mathbf{A} = \begin{bmatrix} \mathbf{S}_0^{(0)} & 1 & \dots & \dots & 0 \\ 1 & -\mathbf{S}_0^{(1)} & -1 & \dots & \vdots \\ \vdots & -1 & \mathbf{S}_0^{(2)} & \dots & \vdots \\ \vdots & \vdots & \vdots & \ddots & \pm 1 \\ 0 & \dots & \dots & \pm 1 & \pm\mathbf{S}_0^{(M)} \end{bmatrix}, \quad \mathbf{B} = \begin{bmatrix} \mathbf{S}_1^{(0)} & 0 & \dots & \dots & 0 \\ 0 & -\mathbf{S}_1^{(1)} & 0 & \dots & \vdots \\ \vdots & 0 & \mathbf{S}_1^{(2)} & \dots & \vdots \\ \vdots & \vdots & \vdots & \ddots & 0 \\ 0 & \dots & \dots & 0 & \pm\mathbf{S}_1^{(M)} \end{bmatrix}$$

$$[\hat{\mathbf{u}}]^T = [\hat{\mathbf{u}}_c \quad \hat{\mathbf{v}}_1 \quad \hat{\mathbf{v}}_2 \quad \dots \quad \hat{\mathbf{v}}_M]^T, \quad [\hat{\mathbf{f}}]^T = [\hat{\mathbf{f}}_c \quad 0 \quad 0 \quad \dots \quad 0]^T \tag{20}$$

4. Numerical example

A coupled system with gyroscopic rotors, foundation plate and soil is discussed as a practical example. The rotor with a 4 [m] shaft's length as shown in Fig. 2 is considered an unbalance excitation source and is supported by bearings mounted on the concrete foundation plate. The bearing stiffness and damping coefficients are provided by Lund and Thomsen (1978) which are presented in Suarez *et al.* (1992). These coefficients are taken as constant values independent of the spin speed of the rotor. Details of the rotor properties are shown in Tables 1 and 2. Here, r_{ds} and h_{ds} are disk's diameter and thickness, respectively. J_p and J_r are the disk's moment inertia about the rotation axis x and any other axis in the disk plane (y, z), respectively.

Table 1 Properties of rotor in Fig. 2

Poisson's ratio ν	=	0.3
Young's Modulus E	=	2.08×10^{11} [N/m^2]
Shear Modulus G	=	7.99×10^{10} [N/m^2]
Mass ρ	=	7806 [kg/m^3]
Shaft diameter r_{sh}	=	0.19 [m]

Bearing stiffness coefficients [N/m]:
$K_{yy}^b = 1.8305 \times 10^8$, $K_{zz}^b = 1.0977 \times 10^8$

Bearing damping coefficients [N s/m]:
$D_{yy}^b = 5.4139 \times 10^6$, $D_{zz}^b = 2.1294 \times 10^6$

Table 2 Disk's properties of rotor in Fig. 2

Disk	r_{ds} [m]	h_{ds} [m]	m [kg]	J_p [kg m^2]	J_r [kg m^2]	ε [m]
D1	0.435	0.125	580.052	54.880	28.195	5.75×10^3
D2	0.650	0.160	1657.773	350.205	178.639	1.05×10^2
D3	0.650	0.160	1657.773	350.205	178.639	1.05×10^2

(a) 3d view

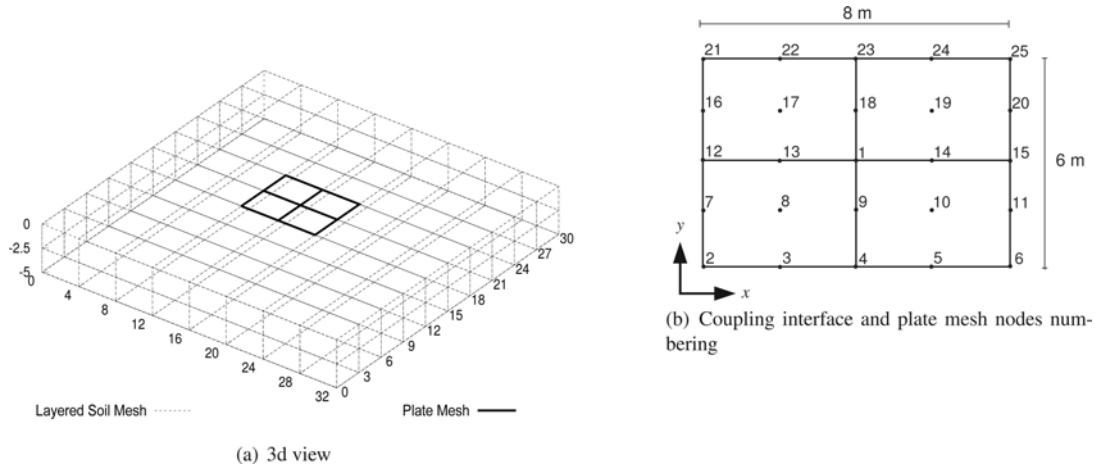(b) Coupling interface and plate mesh nodes numbering

Fig. 3 Elastic foundation plate of rotor in Fig. 2 on a soft clay soil mesh

The coupling interface between soil and foundation plate is treated as an elastic connection. The rotor and the foundation plate are resting on a soft clay soil layer with depth $d = 5.0$ [m] over rigid bedrock as shown in Fig. 2. This soft clay soil parameters are shear modulus $G = 2.1 \times 10^6$ [N/m^2], mass per volume $\rho = 1500$ [kg/m^3] and poisson ratio $\nu = 0.44$. The foundation plate properties are Young's modulus $E = 2.1 \times 10^{10}$ [N/m^2], poisson's ratio $\nu_{pl} = 0.2$ and mass $\rho_{pl} = 2450$ [kg/m^3].

The foundation plate size is 8×6 [m^2] with thickness $h = 68$ [cm]. The problem discretization mesh is shown in Fig. 3 and is built from 232 isoparametric elements with 930 nodes.

The soil dynamical stiffness $\mathbf{K}$ is established by means of an approximation of order $M = 4$,

$$\mathbf{K} \approx [\mathbf{Q}]^{-1}[\mathbf{P}]$$
$$= [\mathbf{Q}_0 + i\omega\mathbf{Q}_1 + \ldots + (i\omega)^4\mathbf{Q}_5]^{-1}[\mathbf{P}_0 + i\omega\mathbf{P}_1 + \ldots + (i\omega)^5\mathbf{P}_6]$$

(21)

(a) Vertical stiffness K_{vv}; node 1

(b) Horizontal stiffness K_{hh-1}; node 1
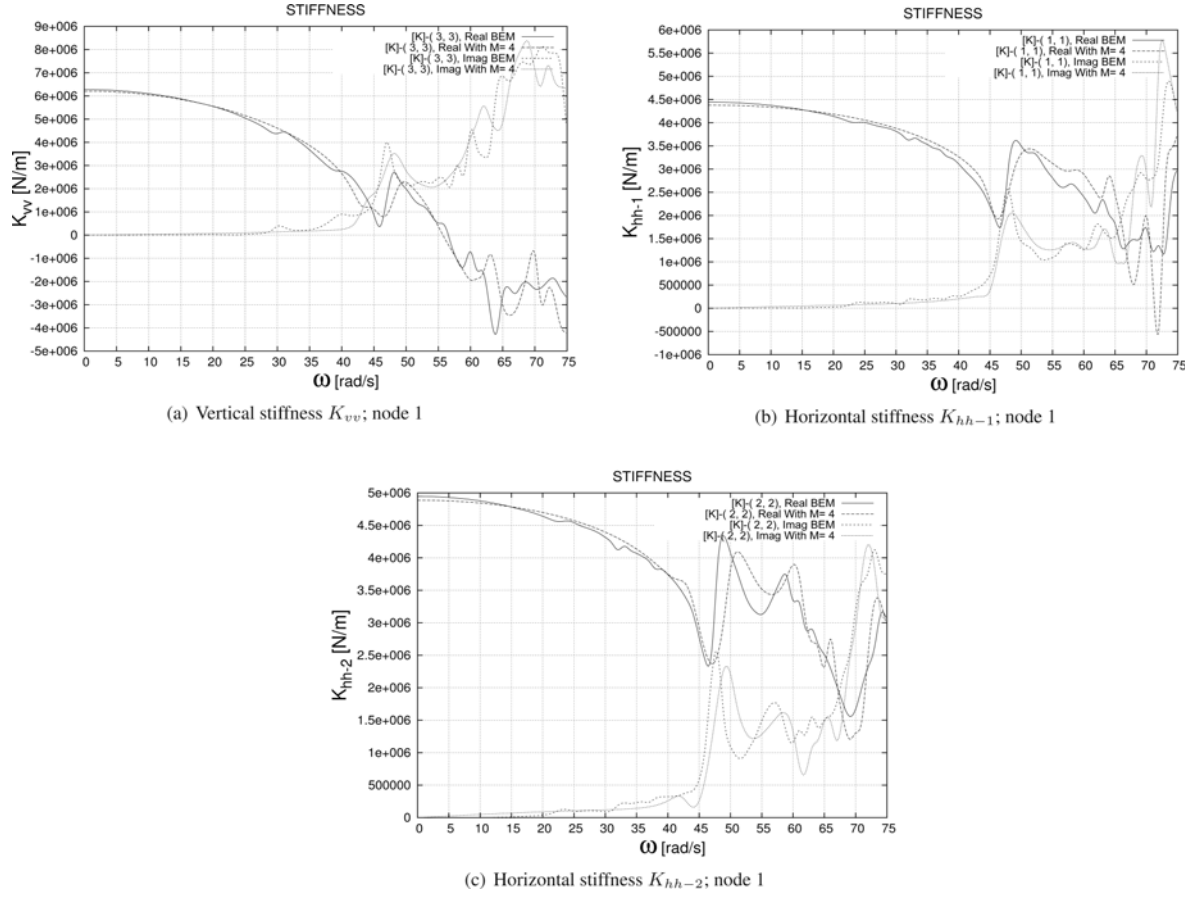
(c) Horizontal stiffness K_{hh-2}; node 1

Fig. 4 Soil stiffness approximation at the center of coupling interface (node 1). Soil properties: $G = 2.1 \times 10^6$ [N/m^2], $\rho = 1500$ [kg/m^3] and $\nu = 0.44$. Rigid bedrock at depth $d = 5$ [m]

The least square process uses 76 input values of $\mathbf{K}(\omega_j)$ as a result of the boundary element method. The boundary element method is performed in the frequency range from $\omega_1 = 0.0$ [rad/s] to $\omega_{76} = 75.0$ [rad/s] with the increment of $\Delta\omega = 1.0$ [rad/s].

The resulting soil dynamical stiffness and its corresponding approximation at the center of the coupling interface (node 1) is shown in Fig. 4. The approximation results at the other coupling interface locations (nodes 6 and 12) are shown in Fig. 5. The soil dynamical stiffness approximation can be judged as 'good' with this order $M = 4$, since the resulting boundary element method dynamical stiffness itself are already 'wavy' curves.

4.1 Rotor-shaft system

Fig. 6 shows the positive directions of rotations and moments of the rotor-shaft for a single rigid-disk rotor system with a gyroscopic moment M_y (Gasch *et al.* 2002) around the y axis. The angular velocity $\dot{\varphi}_z$ arises when the rigid-disk rotates with angular velocity $\dot{\varphi}_x = -\Omega$.

The equation of motion of this rotor-shaft for a single rigid-disk system with a constant angular acceleration ($\ddot{\varphi}_x = \beta$) can be found in textbooks like (Genta 1995)
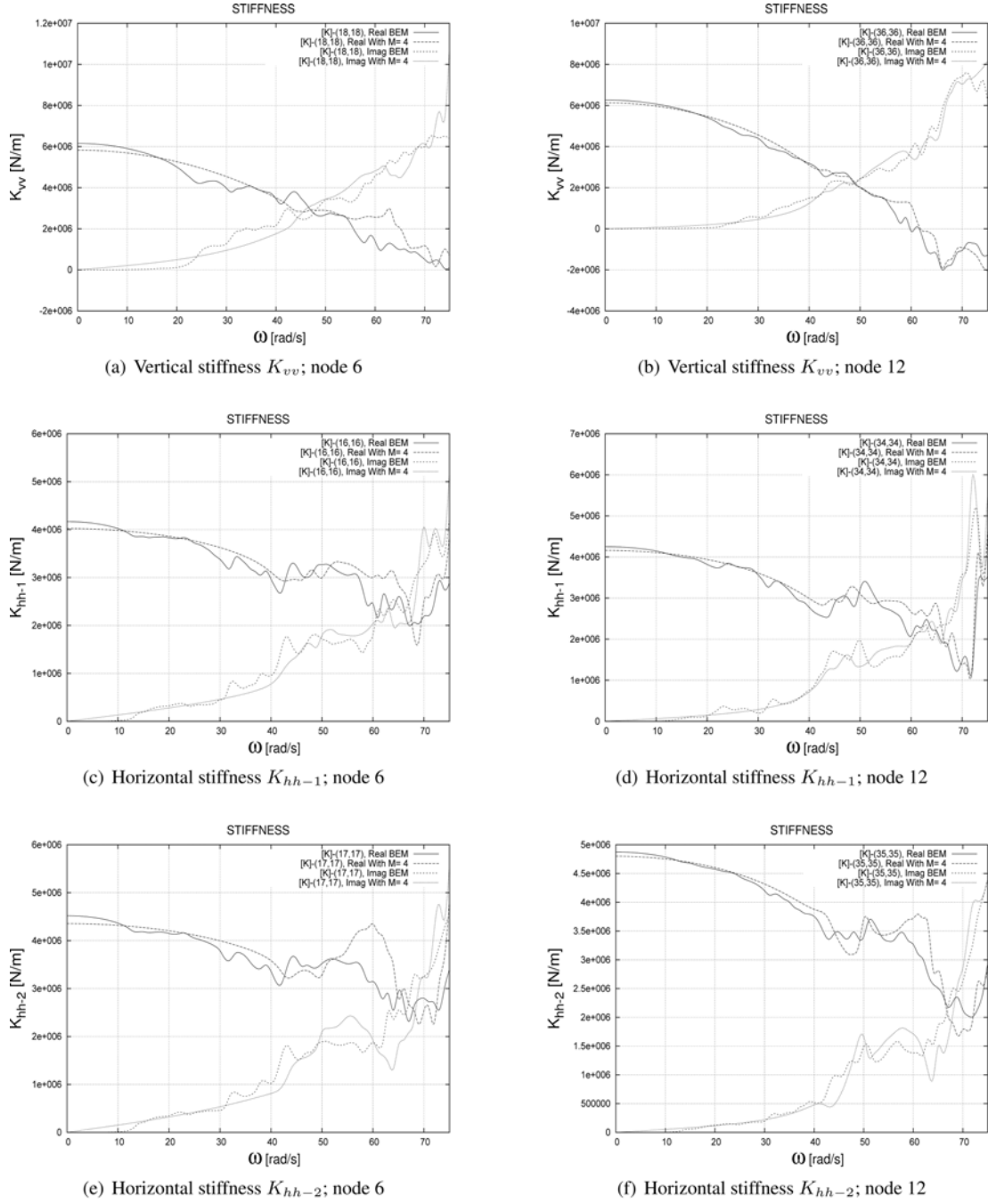
(a) Vertical stiffness K_{vv}; node 6

(b) Vertical stiffness K_{vv}; node 12

(c) Horizontal stiffness K_{hh-1}; node 6

(d) Horizontal stiffness K_{hh-1}; node 12

(e) Horizontal stiffness K_{hh-2}; node 6

(f) Horizontal stiffness K_{hh-2}; node 12

Fig. 5 Soil stiffness approximation at node 6 and node 12 at the coupling interface. Soil properties: $G = 2.1 \times 10^6$ [N/m^2], $\rho = 1500$ [kg/m^3] and $\nu = 0.44$. Rigid bedrock at depth $d = 5$ [m]
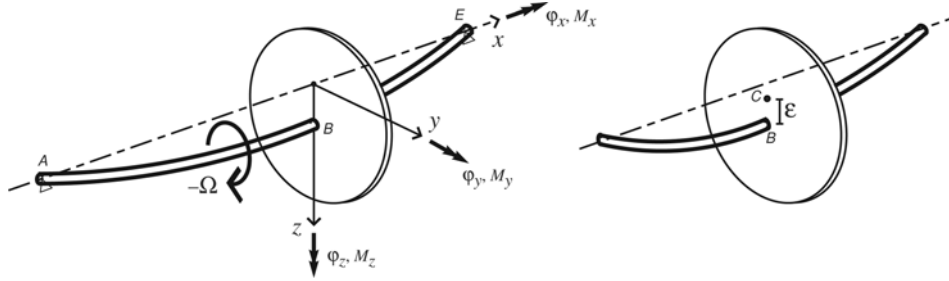
Fig. 6 Shaft with a single rigid-disk with positive rotations and moments

$$\begin{bmatrix} m & 0 & & \\ 0 & J_R & & \\ & & m & 0 \\ & & 0 & J_R \end{bmatrix} \begin{bmatrix} \ddot{z}_{ds} \\ \ddot{\varphi}_{ds_y} \\ \ddot{y}_{ds} \\ \ddot{\varphi}_{ds_z} \end{bmatrix} = \begin{bmatrix} & & 0 & 0 \\ & & 0 & -\dot{\varphi}_x J_P \\ 0 & 0 & & \\ 0 & \dot{\varphi}_x J_P & & \end{bmatrix} \begin{bmatrix} \dot{z}_{ds} \\ \dot{\varphi}_{ds_y} \\ \dot{y}_{ds} \\ \dot{\varphi}_{ds_z} \end{bmatrix} + \begin{bmatrix} c_{11} & c_{12} & & \\ c_{21} & c_{22} & & \\ & & c_{11} & -c_{12} \\ & & -c_{21} & c_{22} \end{bmatrix} \begin{bmatrix} z_{sh} \\ \varphi_{sh_y} \\ y_{sh} \\ \varphi_{sh_z} \end{bmatrix} =$$

$$\begin{bmatrix} m\varepsilon\{\ddot{\varphi}_x \sin(\varphi_x) + \dot{\varphi}_x^2 \cos(\varphi_x)\} \\ 0 \\ m\varepsilon\{-\ddot{\varphi}_x \cos(\varphi_x) + \dot{\varphi}_x^2 \sin(\varphi_x)\} \\ 0 \end{bmatrix}, \tag{22}$$

$$\Rightarrow [\mathbf{M}^r]\ddot{\mathbf{u}}_r + [\mathbf{G}^r(\dot{\varphi}_x)]\dot{\mathbf{u}}_r + [\mathbf{K}^r]\mathbf{u}_r = \mathbf{f}_{r\beta} \tag{23}$$

Subscripts *sh* and *ds* in (22) denote for shaft element and disk element, respectively. The values c_{ij} in the above equation describe stiffnesses of the shaft element

$$c_{11} = \frac{12EI}{\ell^3}, \ c_{12} = c_{12} = \frac{6EI}{\ell^2}, \ c_{22} = \frac{4EI}{\ell^3}, \text{ with } \ell = \text{shaft's length}.$$

The right side of Eq. (22) is caused by the eccentricity ε between the center of gravity of the rigid disk (*C*) and the center of the shaft element (*B*) as shown in Fig. 6.

The rotor in Fig. 2 is accelerated by a constant angular acceleration $\beta = 1.75$ [rad/s²] with respect to time as shown in Fig. 7 and thus generates unbalanced excitations for the foundation plate. The rotor's constant operating spin speed is $\Omega = 17.5$ [rad/s] ≈ 167 [rpm] in the interval $t_1 \le t \le t_2$. The rotor is mounted on the foundation plate by bearings at nodes 13 and 14 which are shown in
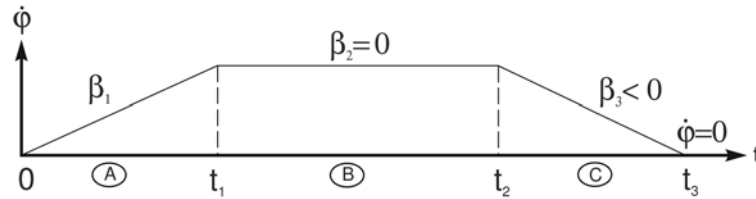

Fig. 7 Disk angular acceleration β with respect to time

Fig. 3(b). Details φ, $\dot{\varphi}$ and $\ddot{\varphi}$ due to the angular acceleration β with respect to time as shown in Fig. 7 are described in appendix A.

The equation of motion of the rotor-foundation-soil problem in this example can be written as

$$\mathbf{A}\mathbf{u} + \mathbf{B}(\dot{\varphi}_x)\dot{\mathbf{u}} + \mathbf{C}\ddot{\mathbf{u}} = \mathbf{f}_{r\beta} \tag{24}$$

where $\dot{\varphi}_x$ is the angular velocity of rotor due to a constant angular acceleration β. $\mathbf{f}_{r\beta}$ is the total rotor unbalanced load from rigid disks element, i.e., the right side matrix of Eq. (22) for each rigid disk of rotor.

A more detailed representation of Eq. (24) contains the displacements $\mathbf{u}_{cp}$ in the coupling interface, the additional variables $\mathbf{v}$ and the displacements $\mathbf{u}_r$ of the rotor. In addition, the second order system in (24) is expanded to a first order system by additional state variables

$$\mathbf{y}_{cp} = \dot{\mathbf{u}}_{cp}, \quad \mathbf{y}_r = \dot{\mathbf{u}}_r \tag{25}$$

$$\begin{bmatrix} \mathbf{A}_{11}+\mathbf{K}_{pl} & \mathbf{A}_{12} & \mathbf{0} \\ \mathbf{A}_{21} & \mathbf{A}_{22} & \mathbf{0} \\ \mathbf{0} & \mathbf{0} & \mathbf{K}^r \end{bmatrix}\begin{bmatrix} \mathbf{u}_{cp} \\ \mathbf{v} \\ \mathbf{u}_r \end{bmatrix} + \begin{bmatrix} \mathbf{B}_{11} & \mathbf{B}_{12} & \mathbf{0} \\ \mathbf{B}_{21} & \mathbf{B}_{22} & \mathbf{0} \\ \mathbf{0} & \mathbf{0} & \mathbf{G}^r(\dot{\varphi}_x) \end{bmatrix}\begin{bmatrix} \mathbf{y}_{cp} \\ \mathbf{v} \\ \mathbf{y}_r \end{bmatrix} + \begin{bmatrix} \mathbf{C} & \mathbf{0} & \mathbf{0} \\ \mathbf{0} & \mathbf{0} & \mathbf{0} \\ \mathbf{0} & \mathbf{0} & \mathbf{M}^r \end{bmatrix}\begin{bmatrix} \dot{\mathbf{y}}_{cp} \\ \mathbf{0} \\ \dot{\mathbf{y}}_r \end{bmatrix} = \begin{bmatrix} \mathbf{0} \\ \mathbf{0} \\ \mathbf{0} \end{bmatrix} \tag{26}$$

where
$\mathbf{A}$ and $\mathbf{B}$: matrices of the soil system,
$\mathbf{K}_{pl}$: bending plate stiffness matrix,
$\mathbf{C}$: bending plate mass matrix,
$\mathbf{K}^r$: rotor stiffness matrix,
$\mathbf{G}^r$: rotor gyroscopic matrix,
$\mathbf{M}^r$: rotor mass matrix.

The foundation plate in this paper is analyzed by using Mindlin's plate theory presented in Cook *et al.* (1989). The consistent mass matrix of the bending plate element is defined as

$$[\mathbf{m}] = \int_V \rho_{pl}[\mathbf{N}]^T[\mathbf{N}]dV \tag{27}$$

where ρ_{pl} and $\mathbf{N}$ are plate mass per volume and shape functions of the quadratic Mindlin plate element, respectively.

Rearranging (25) and (26) yields the rotor-foundation-soil equation of motion

$$\begin{bmatrix} 1 & 0 & 0 & 0 & 0 \\ 0 & -(\mathbf{A}_{11}+\mathbf{K}_{pl}) & -\mathbf{A}_{12} & 0 & 0 \\ 0 & -\mathbf{A}_{21} & -\mathbf{A}_{22} & 0 & 0 \\ 0 & 0 & 0 & 1 & 0 \\ 0 & 0 & 0 & 0 & -\mathbf{K}^r \end{bmatrix}\begin{bmatrix} \mathbf{y}_{cp} \\ \mathbf{u}_{cp} \\ \mathbf{v} \\ \mathbf{y}_r \\ \mathbf{u}_r \end{bmatrix} = \begin{bmatrix} 0 & 1 & 0 & 0 & 0 \\ \mathbf{C} & \mathbf{B}_{11} & \mathbf{B}_{12} & 0 & 0 \\ 0 & \mathbf{B}_{21} & \mathbf{B}_{22} & 0 & 0 \\ 0 & 0 & 0 & 0 & 1 \\ 0 & 0 & 0 & \mathbf{M}^r & \mathbf{G}^r(\dot{\varphi}_x) \end{bmatrix}\begin{bmatrix} \dot{\mathbf{y}}_{cp} \\ \dot{\mathbf{u}}_{cp} \\ \mathbf{v} \\ \dot{\mathbf{y}}_r \\ \dot{\mathbf{u}}_r \end{bmatrix} \tag{28}$$

Expanding the rotor equation of motion in (28) with the additional matrices from the rotor bearings leads to the final rotor-foundation-soil equation of motion in a state space form

$$
\begin{bmatrix}
1 & 0 & 0 & 0 & 0 & 0 & 0 \\
0 & -\mathbf{A}_{11}+\mathbf{K}_{pl}+\mathbf{K}_{11}^{b\mathrm{A}}+\mathbf{K}_{11}^{b\mathrm{B}} & -\mathbf{A}_{12} & 0 & 0 & -\mathbf{K}_{12}^{b\mathrm{A}} & -\mathbf{K}_{12}^{b\mathrm{B}} \\
0 & -\mathbf{A}_{21} & -\mathbf{A}_{22} & 0 & 0 & 0 & 0 \\
0 & 0 & 0 & 1 & 0 & 0 & 0 \\
0 & 0 & 0 & 0 & 1 & 0 & 0 \\
0 & -\mathbf{K}_{21}^{b\mathrm{A}} & 0 & 0 & 0 & -\mathbf{K}_{11}^{r}+-\mathbf{K}_{22}^{b\mathrm{A}} & -\mathbf{K}_{12}^{r} \\
0 & -\mathbf{K}_{21}^{b\mathrm{B}} & 0 & 0 & 0 & -\mathbf{K}_{21}^{r} & -\mathbf{K}_{22}^{r}+-\mathbf{K}_{22}^{b\mathrm{B}}
\end{bmatrix}_{[\bar{\mathbf{A}}]}
\begin{bmatrix}
\mathbf{y}_{cp} \\ \mathbf{u}_{cp} \\ \mathbf{v} \\ \mathbf{y}_{r1} \\ \mathbf{y}_{r2} \\ \mathbf{u}_{r1} \\ \mathbf{u}_{r2}
\end{bmatrix}_{[\mathbf{v}]} =
$$

$$
\begin{bmatrix}
0 & 1 & 0 & 0 & 0 & 0 & 0 \\
\mathbf{C} & \mathbf{B}_{11}+\mathbf{D}_{11}^{b\mathrm{A}}+\mathbf{D}_{11}^{b\mathrm{B}} & \mathbf{B}_{12} & 0 & 0 & \mathbf{D}_{12}^{b\mathrm{A}} & \mathbf{D}_{12}^{b\mathrm{B}} \\
0 & \mathbf{B}_{21} & \mathbf{B}_{22} & 0 & 0 & 0 & 0 \\
0 & 0 & 0 & 0 & 0 & 1 & 0 \\
0 & 0 & 0 & 0 & 1 & 0 & 0 \\
0 & \mathbf{D}_{21}^{b\mathrm{A}} & 0 & \mathbf{M}_{11}^{r} & \mathbf{M}_{12}^{r} & \mathbf{G}_{11}^{r}+\mathbf{D}_{22}^{b\mathrm{A}} & \mathbf{G}_{12}^{r} \\
0 & \mathbf{D}_{21}^{b\mathrm{B}} & 0 & \mathbf{M}_{21}^{r} & \mathbf{M}_{22}^{r} & \mathbf{G}_{21}^{r} & \mathbf{G}_{22}^{r}+\mathbf{D}_{22}^{b\mathrm{B}}
\end{bmatrix}_{[\bar{\mathbf{B}}]}
\begin{bmatrix}
\dot{\mathbf{y}}_{cp} \\ \dot{\mathbf{u}}_{cp} \\ \mathbf{v} \\ \dot{\mathbf{y}}_{r1} \\ \dot{\mathbf{y}}_{r2} \\ \dot{\mathbf{u}}_{r1} \\ \mathbf{u}_{r2}
\end{bmatrix}_{[\dot{\mathbf{v}}]}
$$

$$\Rightarrow [\bar{\mathbf{A}}][\mathbf{v}] = [\bar{\mathbf{B}}][\dot{\mathbf{v}}] \tag{29}$$

where $\mathbf{K}^b$ and $\mathbf{D}^b$ are the stiffness and damping matrix of the bearing support between rotor-shaft and the foundation respectively.

The stiffness and damping matrices of the rotor bearing support are

$$
\mathbf{K}^b = \left[\begin{array}{c|c} \mathbf{K}_{11}^b & \mathbf{K}_{12}^b \\ \hline \mathbf{K}_{21}^b & \mathbf{K}_{22}^b \end{array}\right] =
\left[\begin{array}{c|c|c|c}
K_{yy}^b & 0 & -K_{yy}^b & 0 \\ \hline
0 & K_{zz}^b & 0 & -K_{zz}^b \\ \hline
-K_{yy}^b & 0 & K_{yy}^b & 0 \\ \hline
0 & -K_{zz}^b & 0 & K_{yy}^b
\end{array}\right]
\tag{30}
$$

$$
\mathbf{D}^b = \left[\begin{array}{c|c} \mathbf{D}_{11}^b & \mathbf{D}_{12}^b \\ \hline \mathbf{D}_{21}^b & \mathbf{D}_{22}^b \end{array}\right] =
\left[\begin{array}{c|c|c|c}
D_{yy}^b & 0 & -D_{yy}^b & 0 \\ \hline
0 & D_{zz}^b & 0 & -D_{zz}^b \\ \hline
-D_{yy}^b & 0 & K_{yy}^b & 0 \\ \hline
0 & -D_{zz}^b & 0 & D_{yy}^b
\end{array}\right]
\tag{31}
$$

(a) Vertical displacement u_3 at node 1

(b) Vertical displacement u_3 at node 6

(c) Vertical displacement u_3 at node 13

(d) Vertical displacement u_3 at node 14

(e) Vertical displacement u_3 at node 4

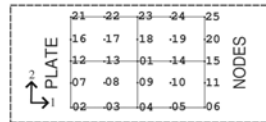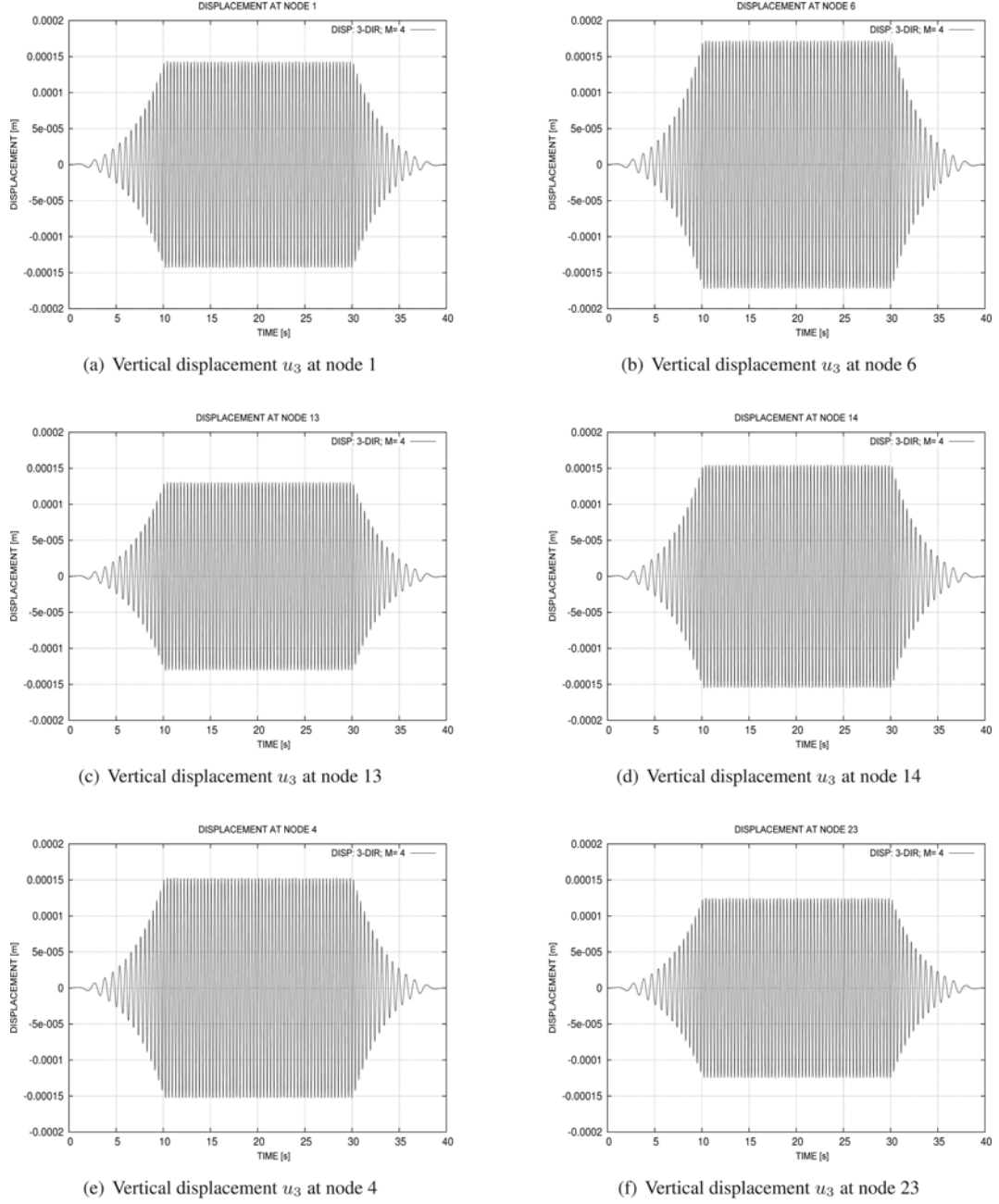(f) Vertical displacement u_3 at node 23

Fig. 8 Vertical displacement u_3 at mass center level of elastic plate due to rotor excitation with $\beta = 1.75$ [rad/s^2]. Soil properties: $G = 2.1 \times 10^6$ [N/m^2], $\rho = 1500$ [kg/m^3] and $\nu = 0.44$. Rigid bedrock at depth $d = 5$ [m].

The structure response due to an unbalance rotor load is determined by solving the Eq. (29) in the time domain due to the load $\mathbf{f}_{r\beta}$ in the Eq. (24)

$$[\overline{\mathbf{A}}][\mathbf{v}] - [\overline{\mathbf{B}}][\dot{\mathbf{v}}] = \mathbf{f}_{r\beta} \qquad (32)$$

The resulting vertical displacements at the foundation plate mass center are shown in Fig. 8. Here, the results are shown only at some plate nodes. These nodes are at the center of plate (node 1), at the plate corner (node 6), at the rotor bearing mountings (nodes 13 and 14) and at the plate edge in y axis direction (nodes 4 and 23).

The displacements amplitude at the rotor constant operating speed ($10[s] < t \le 30[s]$) is checked by solving Eq. (32) due to a load $\hat{\mathbf{f}}_{r\Omega}$ which is the unbalanced load due to the constant rotational speed $\Omega = 17.5$ [rad/s]

$$[\overline{\mathbf{A}} - i\Omega\overline{\mathbf{B}}]\hat{\mathbf{v}} = \hat{\mathbf{f}}_{r\Omega} \qquad (33)$$

where the equation of motion of the rotor-shaft for a single rigid-disk system with a constant angular velocity Ω is taken from Genta (1995)

$$\begin{bmatrix} m & 0 & & \\ 0 & J_R & & \\ & & m & 0 \\ & & 0 & J_R \end{bmatrix}\begin{bmatrix} \ddot{z}_{ds} \\ \ddot{\varphi}_{ds_y} \\ \ddot{y}_{ds} \\ \ddot{\varphi}_{ds_z} \end{bmatrix} = \begin{bmatrix} & & 0 & 0 \\ & & 0 & -\Omega J_P \\ 0 & 0 & & \\ 0 & \Omega J_P & & \end{bmatrix}\begin{bmatrix} \dot{z}_{ds} \\ \dot{\varphi}_{ds_y} \\ \dot{y}_{ds} \\ \dot{\varphi}_{ds_z} \end{bmatrix} + \begin{bmatrix} c_{11} & c_{12} & & \\ c_{21} & c_{22} & & \\ & & c_{11} & -c_{12} \\ & & -c_{21} & c_{22} \end{bmatrix}\begin{bmatrix} z_{sh} \\ \varphi_{sh_y} \\ y_{sh} \\ \varphi_{sh_z} \end{bmatrix} = \Omega^2\begin{bmatrix} m\varepsilon\cos(\Omega t) \\ 0 \\ m\varepsilon\sin(\Omega t) \\ 0 \end{bmatrix} \qquad (34)$$

The right side of the matrix Eq. (33) for each single disk i reads

$$\hat{\mathbf{f}}_{r\Omega} = \Re\{\hat{\mathbf{f}}_{r\Omega}e^{i\Omega t}\} = \Re\left\{\begin{bmatrix} \hat{\mathbf{f}}_{r\Omega_1} \\ \vdots \\ \hat{\mathbf{f}}_{r\Omega_n} \end{bmatrix}e^{i\Omega t}\right\} \quad \text{with} \quad \overline{\mathbf{f}}_r\Omega_i = \begin{bmatrix} \Omega^2 m_i\varepsilon_i \\ 0 \\ -i\Omega^2 m_i\varepsilon_i \\ 0 \end{bmatrix} \qquad (35)$$

The resulting displacement amplitudes are shown in Table 3.

Good agreements are achieved between the resulting amplitudes shown in Table 3 and the displacement amplitudes of the system at rotor constant angular velocity shown in Fig. 8.

The corresponding damping ratio D of the system can roughly determined from the resulting vertical displacement due to an impulse load. Here, a vertical constant load $F = 10^7$ [N] acting at the center of plate with a duration of 0.05 [s] is treated. The resulting vertical displacement at the center of plate (node 1) is shown in Fig. 9.

Table 3 Vertical amplitudes A_{u_3} of rotor displacements at constant angular velocity

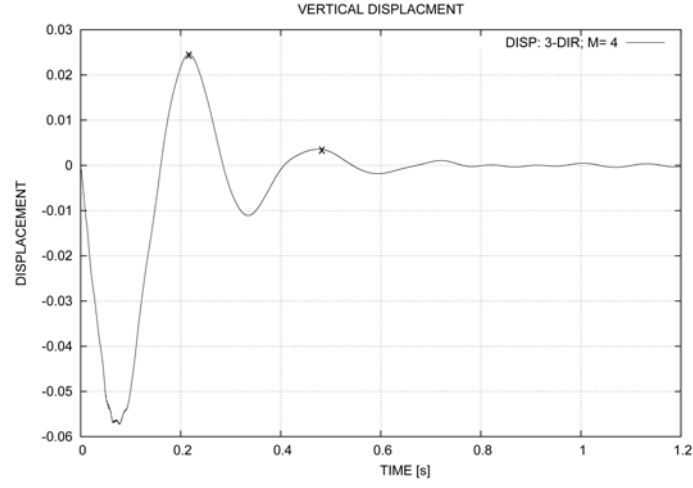| Nodes	01	04	06	13	14	23
A_{u_3} ($\times 10^{-03}$) [m]	0.1159	0.1235	0.1409	0.1050	0.1262	0.1015

Fig. 9 Vertical displacement u_3 at mass center level of elastic plate due to a vertical constant load $F = 10^7$ [N] with a duration of 0.05 [s]. Soil properties: $G = 2.1 \times 10^6$ [N/m^2], $\rho = 1500$ [kg/m^3] and $\nu = 0.44$. Rigid bedrock at depth $d = 5$ [m]

(a) Rotor u_3 amplitudes at center of disk D1 (in figure 2)

(b) Rotor u_3 amplitudes at center of disk D2 (in figure 2)

(c) Rotor u_3 amplitudes at center of disk D3 (in figure 2)
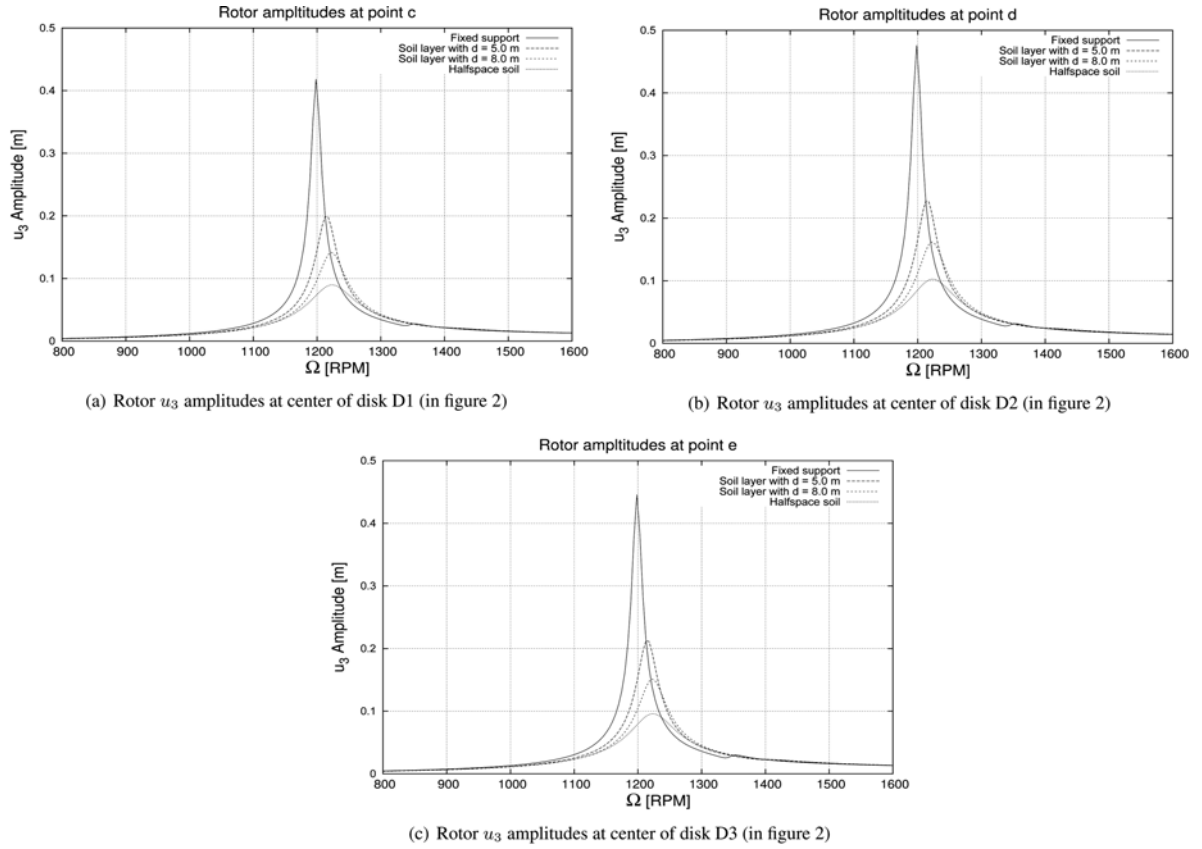
Fig. 10 u_3 Amplitude [m] of the rotor in Fig. 2 at various conditions. Soil properties: $G = 2.1 \times 10^6$ [N/m^2], $\rho = 1500$ [kg/m^3] and $\nu = 0.44$

The logarithmic decrement Λ from the adjacent peak displacements z_1 and z_2 (marked by '*x*') in Fig. 9 reads

$$\Lambda = \ln\left(\frac{z_1}{z_2}\right) = \ln\left(\frac{0.0235}{0.0044}\right) = 1.675$$

Hence, the damping ratio D becomes

$$D \approx \frac{\Lambda}{2\pi} \approx \frac{1.675}{2\pi} = 0.267$$

The next important aspect that is presented here is the influence of the soil layer with respect to radiation damping. This influence is shown by comparing the rotor amplitudes for assuming a rigid soil with the rotor amplitudes for an elastic foundation-soil system. In order to do this, the same gyroscopic rotor of this example is analyzed on various soil depths. Here, the bearing damping coefficient of the rotor D_{yy}^b and D_{zz}^b are reduced to 0.54139×10^5 [N s/m] and 0.21294×10^5 [N s/m], respectively, in order to pronounce the soil radiation damping effect.

Fig. 10 compares the rotor amplitudes for the situation mentioned above. This figure clearly shows the radiation damping effect due to soil presence in the rotor-foundation-soil system.

Obviously, there is a continuous increase of radiation damping when changing from a rigid soil model to a halfspace model.

5. Conclusions

The established rational approximation method in Ruge *et al.* (2001) has been elaborated for coupled system with multiple degrees of freedom. Hence, the coupling between different degrees of freedom is fully preserved. The matrix-valued coefficients of the rational approximation function are determined by means of a least-square procedure. Here, a least-square algorithm for multiple degrees of freedom has been implemented and yields a satisfactory result, particularly concerning the numerical performance. An accurate representation of the soil elastic dynamical stiffness resulting from the boundary element method has been achieved using degrees of rational approximation $M = 4$.

The time-domain representation is achieved by splitting the rational force-displacement into a series of linear functions in the frequency-domain corresponding with first order differential equations in the time-domain. This splitting process has been demonstrated as numerically effective and in addition is characterized by a fully explicit process.

The concept presented in this paper has been successfully used to represent a rotor-foundation-soil problem in a three-dimensional dynamical soil structure interaction analysis for a transient excitation caused by startup and shutdown. The coupling interface between foundation and soil is modeled by a deformable plate. The method presented in this paper demonstrates its performance to deal with this kind of problem which is involving unbounded domains. The important aspect from this rotor-foundation-soil example is the contribution of the radiation damping to the behavior of the system, particularly the rotor response, which is clearly illustrated in Fig. 10. Here, the vertical rotor amplitudes are reduced due to the soil presence in the system, the most reduced amplitudes is given by a soil halfspace. The amount of radiation damping increases with increasing thickness of the soil layer.

References

Ahmad, S. and Banerjee, P.K. (1988), Multi-domain BEM for two-dimensional problems of elastodynamics", *Int. J. Numer. Meth. Eng.*, **26**(4), 891-911. http://dx.doi.org/10.1002/ nme.1620260410 - [Online; last accessed 30-December-2007].

Andersen, L. and Jones, C. (2001), "Three-dimensional elastodynamic analysis using multiple boundary element domains", ISVR Technical Memorandum 867, University of Southampton; Institute Of Sound And Vibration Research, Dynamics Group. http://www.isvr.soton.ac.uk/STAFF/Pubs/Pubpdfs/Pub1370.pdf - [Online; last accessed 30-December-2007].

Antes, H. and Spyrakos, C. (1996), "Soil-structure interaction", In Beskos, D. and Anagnostopoulos, S., editors, *Computer Analysis and Design of Earthquake Resistant Structures. A Handbook*, 271-332. Computational Mechanics Publications, Southampton, UK, Boston, USA.

Bausinger, R. and Kuhn, G. (1987), *Die Boundary-Element-Methode*. Expert Verlag, Stutgart.

Beskos, D.E. (1987), "Boundary element method in dynamic analysis", *Appl. Mech. Rev.*, **40**(1), 1-23.

Cook, R.D., Malkus, D.S. and Plesha, M.E. (1989), *Concepts and Applications of Finite Element Analysis*. John Wiley & Sons, Inc., New York.

Gasch, R., Nordmann, R. and Pfützner, H. (2002), *Rotordynamik*. Springer-Verlag, New York Berlin Heidel-berg, second edition.

Genta, G. (1995), *Vibration of Structures and Machines – Parctical Aspects*, 238-252. Springer-Verlag, New York Berlin Heidelberg, second edition.

Hartmann, F. (1981), "The Somigliana identity on piecewise smooth surfaces", *J. Elast.*, **11**(4), 403-423. http://www.springerlink.com/content/t21m45604rh81831 [Online; last accessed 11-November-2007].

Li, H., Han, G. and Mang, H.A. (1985), "A new method for evaluating singular integrals in stress analysis of solids by the direct boundary element method", *Int. J. Numer. Meth. Eng.*, **21**(11), 2071-2098. http://dx.doi.org/10.1002/nme.1620211109 - [Online; last accessed 30-December-2007].

Lund, J.W. and Thomsen, K.K. (1978), "A calculation method and data for the dynamic coefficients of oil-lubricated journal bearings", In *Topics in Fluid Film Bearing and Rotor Bearing System Design and Optimization*, The Design Engineering Conference, 1-28, Chicago, IL. ASME.

Ruge, P. and Trinks, C. (2002), "Consistent time-domain models for unbounded space-domains", In *Fifth World Conference on Computational Mechanics*, Vienna, Austria.

Ruge, P. and Trinks, C. (2003), "Representation of radiation damping by fractional time derivatives", *Earthq. Eng. Struct. Dyn.*, **32**(7), 1099-1116. http://dx.doi.org/10.1002/eqe.264 - [Online; last accessed 30-December-2007].

Ruge, P., Trinks, C. and Witte, S. (2001), "Time-domain analysis of unbounded media using mixed-variable formulations", *Earthq. Eng. Struct. Dyn.*, **30**(6), 899-925. http://dx.doi.org/10.1002/eqe.47 - [Online; last accessed 30-December-2007].

Ruge, P., Zulkifli, E. and Birk, C. (2006), "Symmetric matrix-valu frequency to time transformation for unbounded domains applied to infinite beams", *Comput. Struct.*, **84**(28), 1815-1826. http://www.sciencedirect.com/science/article/B6V28-4KST3DK-1/2/19ffe521dcbc912e3bcf945f93199fdf - [On-line; last accessed 29-December-2007].

Suarez, L., Singh, M.P. and Rohanimanesh, M.S. (1992), "Seismic response of rotating machines", *Earthq. Eng. Struct. Dyn.*, **21**(1), 21-36. http://dx.doi.org/10.1002/eqe.4290210102.

Trinks, C. (2005), *Consistent Absorbing Boundaries for Time-domain Interaction Analyses Using the Fractional Calculus*. Dissertation, Technische Universität Dresden, Mommsenstr. 13 D-01062 Dresden-Germany.

Trinks, C. and Ruge, P. (2002a), "Description of wave propagation by fading memory", In Grundmann, H. and Schuëller, G. I., editors, *Structural Dynamics – Eurodyn 2002*, 711-716, Munich. Swets & Zeitlinger B.V.

Trinks, C. and Ruge, P. (2002b), "Treatment of dynamic systems with fractional derivatives without evaluating memory-integrals", *Comput. Mech.*, **29**(6), 471-476. http://dx.doi.org/10.1007/s00466-002-0356-5 - [Online; last accessed 30-December-2007].

Trinks, C. and Ruge, P. (2003a), "Dynamic dam-reservoir-interaction - treatment of radiation damping by the mixed-variables technique", *Proc. Appl. Math. Mech.*, **3**(1), 316-317. http://dx.doi.org/10.1002/pamm.200310430 - [Online; last accessed 30-December-2007].

Trinks, C. and Ruge, P. (2003b), "Fractional calculus applied to radiation damping", *Proc. Appl. Math. Mech.*, **2**(1), 266-267. http://dx.doi.org/10.1002/pamm.200310118 - [Online; last accessed 30-December-2007].

Trinks, C., Ruge, P. and Witte, S. (2001a), "Rational approximation of dynamic stiffness matrices for time–domain analysis of unbounded media", *Proc. Appl. Math. Mech.*, **1**(1), 234-235. http://dx.doi.org/10.1002/1617-7061(200203)1:1<234::AID-PAMM234>3.0.CO;2-J - [Online; last accessed 30-December-2007].

Trinks, C., Ruge, P. and Witte, S. (2001b), "Time-domain analysis of unbounded media using rational approximation", In Lin, S., Mao, R., Shen, H., Sun, G. and Sun, Y., editor, *EPMESC VIII – International Conference on Enhancement and Promotion of Computational Methods in Engineering and Science*, Shanghai. San Lian Publisher.

Vaish, A.K. and Chopra, A.K. (1974), "Earthquake finite element analysis of structure-foundation systems", *J. Eng. Mech. Div.*, **100**(6), 1101-1116.

Wolf, J.P. (1991), "Consistent lumped-parmeter models for unbounded soil: physical representation", *Earthq. Eng. Struct. Dyn.*, **20**(1), 11-32. http://dx.doi.org/10.1002/eqe.4290200103 - [Online; last accessed 30-December-2007].

Wolf, J.P. (1994), *Foundation Vibration Analysis Using Simple Physical Model*. Prentice-Hall, Englewood Cliffs, New Jersey, USA.

Zulkifli, E. (2008), *Consistent Description of Radiation Damping in Transient Soil-structure Interaction*. Dissertation, Technische Universität Dresden, Mommsenstr. 13 D-01062 Dresden-Germany. email: Ediansjah.Zulkifli@tu-dresden.de.

A Disk angular acceleration β with respect to time
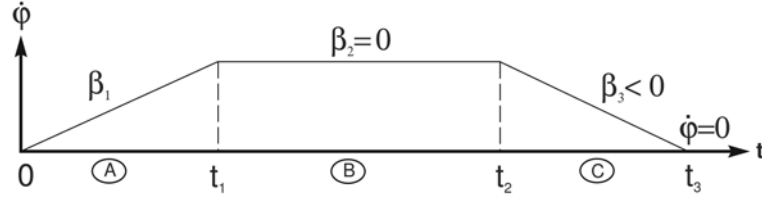
Fig. 11 Disk angular acceleration β with respect to time.

Time interval A $(0 \leq t \leq t_1)$

$t = 0$:

$$\ddot{\varphi} = \beta_1 \ (\text{constant})$$

$$\dot{\varphi} = \omega = \beta_1 t$$

$$\varphi = \frac{\beta_1 t^2}{2}$$

$t = t_1$:

$$\dot{\varphi} = \omega = \beta_1 t_1$$

$$\varphi = \frac{\beta_1 t_1^2}{2}$$

Time interval B $(t_1 \leq t \leq t_2)$

$t = t_1$:

$$\dot{\varphi}_{t_1} = \omega_1 = \beta_1 t_1$$

$$\varphi_{t_1} = \frac{\beta_1 t_1^2}{2}$$

$t_1 < t < t_2$:

$$\ddot{\varphi} = \beta_2 = 0$$

$$\dot{\varphi} = \omega_1 = \beta_1 t_1 \ (\text{constant})$$

$$\varphi = \beta_1 t_1 t + c$$

From the previous interval:

$$\varphi_{t_1} \equiv \frac{\beta_1 t_1^2}{2} = \beta_1 t_1 t_1 + c; \ \rightarrow \ c = -\frac{\beta_1 t_1^2}{2}$$

$$\downarrow$$

$$\varphi = \beta_1 t_1 \left(t - \frac{t_1}{2} \right)$$

$t = t_2$:

$$\dot{\varphi} = \omega_2 = \beta_1 t_1$$

$$\varphi = \beta_1 t_1 \left(t_2 - \frac{t_1}{2} \right)$$

Time interval C $(t_2 \le t \le t_3)$

$t = t_2$:

$$\dot{\varphi}_{t_2} = \beta_1 t_1$$

$$\varphi_{t_2} = \beta_1 t_1 \left(t_2 - \frac{t_1}{2} \right)$$

$t_2 < t < t_3$:

$$\ddot{\varphi} = \beta_3 \ (\text{constant})$$

$$\dot{\varphi} = \beta_3 t + c_1$$

$$\varphi = \frac{\beta_3 t^2}{2} + c_1 t + c_2$$

From the previous interval:

$$\dot{\varphi}_{t_2} \equiv \beta_1 t_1 = \beta_3 t_2 + c_1; \ \rightarrow \ c_1 = \beta_1 t_1 - \beta_3 t_2$$

$$\varphi_{t_2} \equiv \beta_1 t_1 \left(t_2 - \frac{t_1}{2} \right) = \frac{\beta_3 t_2^2}{2} + c_1 t_2 + c_2; \ \rightarrow \ c_2 = \frac{\beta_3 t_2^2}{2} - \frac{\beta_1 t_1^2}{2}$$

$$\downarrow$$

$$\dot{\varphi} = \beta_3 t + \beta_1 t_1 - \beta_3 t_2$$

$$\varphi = \frac{\beta_3 t^2}{2} + (\beta_1 t_1 - \beta_3 t_2) t + \left(\frac{\beta_3 t_2^2}{2} - \frac{\beta_1 t_1^2}{2} \right)$$

$t = t_3$:

$$\dot{\varphi} = 0 \rightarrow \beta_3 t_3 + \beta_1 t_1 - \beta_3 t_2 = 0 \rightarrow t_3 = \frac{-\beta_1 t_1 + \beta_3 t_2}{\beta_3}$$